ACS APPLIED MATERIALS & INTERFACES

Research Article

Cite This: ACS Appl. Mater. Interfaces 2017, 9, 36053-36060

www.acsami.org

Accomplishment of Multifunctional π-Conjugated Polymers by Regulating the Degree of Side-Chain Fluorination for Efficient Dopant-Free Ambient-Stable Perovskite Solar Cells and Organic Solar Cells

Kakaraparthi Kranthiraja,[†] Sang Ho Park,[†] Hyunji Kim,[†] Kumarasamy Gunasekar,[†] Gibok Han,[‡] Bumjoon J. Kim,[‡] Chang Su Kim,[§] Soohyun Kim,[∥] Hyunjung Lee,*[,∥] Ryosuke Nishikubo,[⊥] Akinori Saeki,*[,⊥] Sung-Ho Jin,*[,†] and Myungkwan Song*[,§]

[†]Department of Chemistry Education, Graduate Department of Chemical Materials, Institute for Plastic Information and Energy Materials, Pusan National University, Busan 46241, Korea

[‡]Department of Chemical and Biomolecular Engineering, Korea Advanced Institute of Science and Technology (KAIST), Daejeon 305-701, Korea

[§]Surface Technology Division, Korea Institute of Materials Science, Changwon 641-831, Korea

[∥]School of Advanced Materials Engineering, Kookmin University, Seoul 136-702, Korea

[⊥]Department of Applied Chemistry, Graduate School of Engineering, Osaka University, Osaka 565-0871, Japan

Supporting Information

ABSTRACT: We present an efficient approach to develop a series of multifunctional π-conjugated polymers (P1−P3) by controlling the degree of fluorination (0F, 2F, and 4F) on the side chain linked to the benzodithiophene unit of the π-conjugated polymer. The most promising changes were noticed in optical, electrochemical, and morphological properties upon varying the degree of fluorine atoms on the side chain. The properly aligned energy levels with respect to the perovskite and PCBM prompted us to use them in perovskite solar cells (PSCs) as hole-transporting materials (HTMs) and in bulk heterojunction organic solar cells (BHJ OSCs) as photoactive donors. Interestingly, P2 (2F) and P3 (4F) showed an enhanced power conversion efficiency (PCE) of 14.94%, 10.35% compared to P1 (0F) (9.80%) in dopant-free PSCs. Similarly, P2 (2F) and P3 (4F) also showed improved PCE of 7.93% and 7.43%, respectively, compared to P1 (0F) (PCE of 4.35%) in BHJ OSCs. The high photvoltaic performance of the P2 and P3 based photovotaic devices over P1 are well correlated with their energy level alignment, charge transporting, morphological and packing properties, and hole transfer yields. In addition, the P1−P3 based dopant-free PSCs and BHJ OSCs showed an excellent ambient stability up to 30 days without a significant drop in their initial performance.

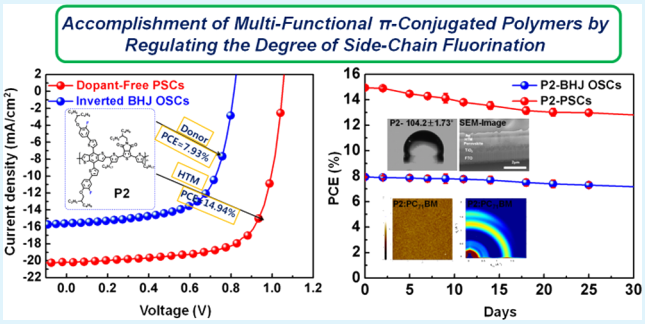

KEYWORDS: *multifunctional π-conjugated polymers, efficient dopant-free perovskite solar cells, efficient organic solar cells, long-term stability, time-resolved microwave conductivity*

INTRODUCTION

The exploration of renewable light-harvesting technologies including perovskite solar cells (PSCs) and bulk heterojunction organic solar cells (BHJ OSCs) has attracted significant academic attention due to their fascinating features such as solution processability, flexibility, and large area devices for the next-generation solar cell technologies.[1−9] The power conversion efficiency (PCE) of PSCs has been dramatically improved by over 22% by amending the electronic quality of perovskite and by using state-of-the-art hole-transporting materials (HTMs) such as tetrakis(*N*,*N*-di-*p*-methoxyphenylamine)-9,9′-spirobifluorene (spiro-OMeTAD) owing to its enhanced charge transport toward the electrode via properly aligned energy levels with respect to the perovskite.[10] Similarly, BHJ OSCs have recently attained a high PCE over 12% by careful engineering of the molecular structure of photoactive donors and systematic device optimization.[11] Therefore, the roles of overlaying HTMs in PSCs and photoactive donors of BHJ OSCs have become essential for optimizing or improving the PCE and long-term stability. Despite being the benchmark

Received: June 26, 2017
Accepted: September 26, 2017
Published: September 26, 2017

Downloaded via KOOKMIN UNIV on July 10, 2019 at 07:50:37 (UTC).
See https://pubs.acs.org/sharingguidelines for options on how to legitimately share published articles.

© 2017 American Chemical Society

DOI: 10.1021/acsami.7b09146
ACS Appl. Mater. Interfaces 2017, 9, 36053−36060

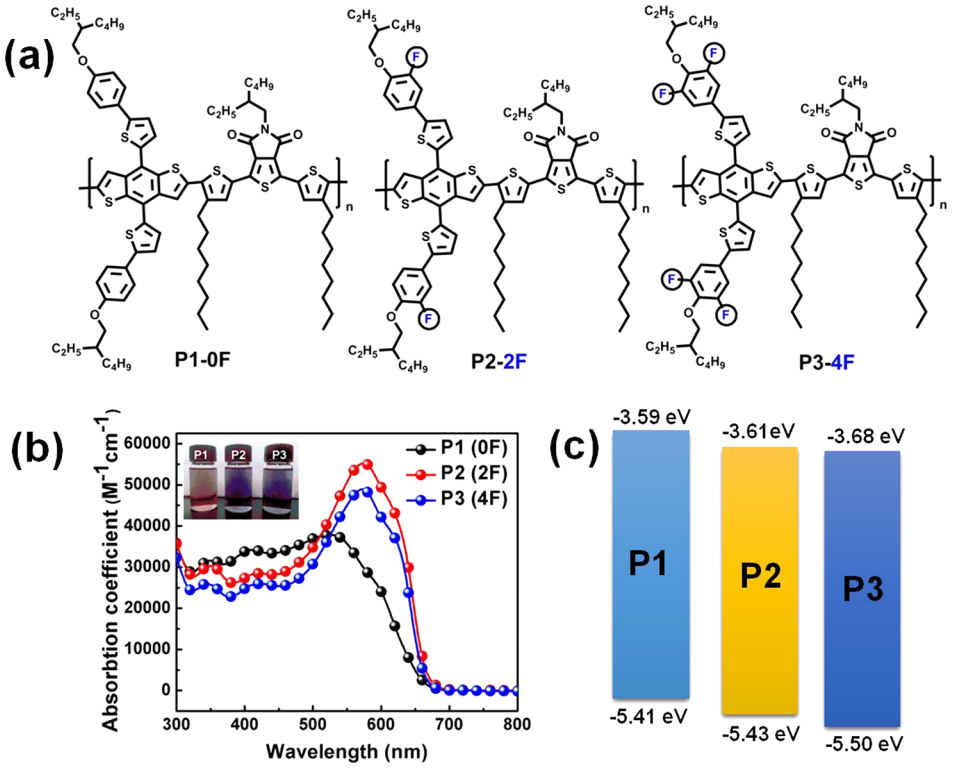

Figure 1. (a) Molecular structures of P1−P3. (b) Absorption coefficient spectra of P1−P3. (c) Energy level diagram of P1−P3.

HTM, the conventional HTM (spiro-OMeTAD) in its pristine form has been suffering from poor mobility and conductivity and, thus, typically requires p-type doping that could cause serious stability issues in the device and restrict its practical use.[12,13] Therefore, replacing the spiro-OMeTAD with new HTMs with the desired properties of appropriate energy levels, high hole mobility in its pristine form, low cost, and easy processable materials is necessary for attaining highly efficient and stable PSCs, which are anticipated to be truly compatible for practical application.

In this regard, π-conjugated polymers are potential alternatives to small-molecule HTMs due to their attractive features such as high hole mobility, hydrophobicity, quality film patterns without pinholes, lower material consumption, and passivation of the perovskite layer.[14−18] Despite the considerable advances in the development of alternative planar small-molecule HTMs in place of conventional meso-structured propeller-type materials (spiro-OMeTAD),[19−21] not much progress has been made in π-conjugated polymer-based based HTMs for PSCs. In addition, most of the existing polymer-based HTMs showed poor performances in their pristine form, and also, most of them need p-type doping to attain high device performance.[22−25] Similarly, few thiophene-based polyelectrolytes have been reported with high performance, but their hygroscopic nature will affect the device stability by a corroding perovskite layer.[25] Moreover, these external dopants can complicate the device optimization process, compromise the device stability, and increase the overall production cost. Recently, few research groups have successfully demonstrated the real potential behavior of polymer HTMs in achieving high performance dopant-free PSCS with long-term stability, but their role only limited as HTMs in PSCs, and their compatibility in BHJ OSCs has not been explored.[26,27] Recently, we successfully demonstrated the potential compatibility of conjugated polymers for multiple applications with great performance in both PSCs and BHJ OSCs.[28] Therefore, the development of new polymer HTMs with intrinsically rich optoelectronic properties not only enhances the current PCE of PSCs but also can be extended to BHJ OSCs as photoactive donors.

Until now, the fluorine substitution on the donor−acceptor (D−A) π-conjugated polymer backbone has been widely investigated as a successful approach for simultaneously enhancing photovoltaic properties in BHJ OSCs. Unfortunately, the direct fluorination on the BDT unit showed detrimental impact on electrical and morphological properties and resulted in poor performance.[29] In contrast to that, our side-chain fluorination approach has many significant merits compared to direct fluorination on the BDT unit.[30] However, no systematic investigations have been undertaken on the degree of side-chain fluorination in π-conjugated polymer HTMs and its impact on PSCs. Furthermore, regulating the degree of side-chain fluorination in π-conjugated polymers will assist in developing efficient photoactive donors for high performance BHJ OSCs. Herein, we report a series of multifunctional π-conjugated polymers (P1 (0F), P2 (2F), and P3 (4F)) with different number of fluorine atoms in the conjugated side chain linked to benzodithiophene to explore the correlation between the degree of fluorine content in the π-conjugated polymers and the photovoltaic properties of the resulting dopant-free PSCs and BHJ OSCs. The key monomers and polymers (Scheme S1) in the study were synthesized according to our recent report.[30] We presumed that P1−P3 with different degrees of fluorine substitution on the 2D-conjugated side chain would improve the charge transport behaviors via enhanced inter/intramolecular interactions through strong $\pi-\pi$ stacking, vary the lifetime of the charge-separated excited state, and increase the hydrophobicity of

DOI: 10.1021/acsami.7b09146
ACS Appl. Mater. Interfaces 2017, 9, 36053−36060

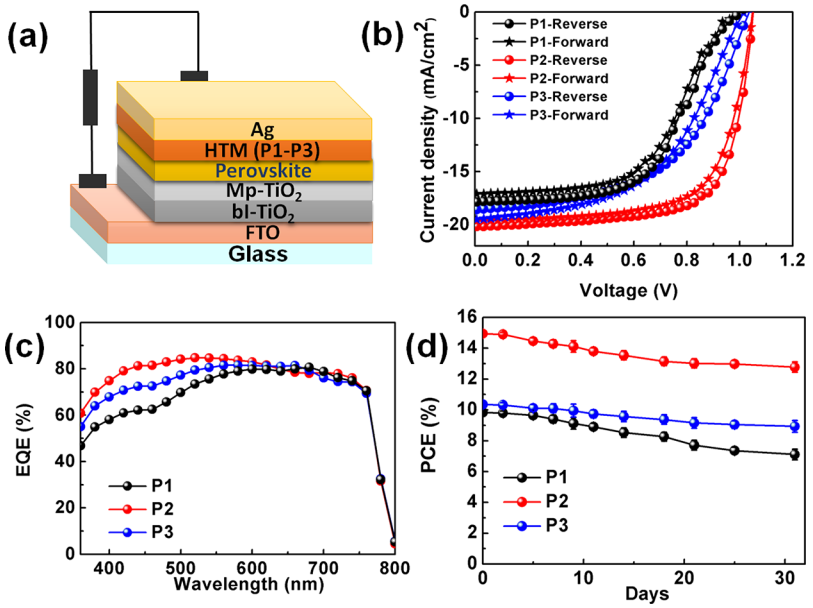

Figure 2. (a) Device structure of PSCs. (b) *J*−*V* curves of P1−P3-based PSCs. (c) EQE curves of P1−P3-based PSCs. (d) Stability of P1−P3-based PSCs.

polymers, which will affect the performance and long-term stability of dopant-free PSCs and BHJ OSCs. Upon placing the new polymers (P1−P3) in dopant-free PSCs as HTMs, we observed significant differences in their photovoltaic properties with respect to the fluorine content in the π-conjugated polymers. In particular, the fluorinated polymers P2 and P3 showed enhanced photovoltaic performance (maximum PCE of 14.94% and 10.35%) compared to the nonfluorinated polymer P1 (maximum PCE of 9.80%) without any external dopants, which are far superior than spiro-OMeTAD-based dopant-free PSC performance (PCE = 8.74%). Similarly, P2 and P3 showed excellent compatibility with $PC_{71}BM$ and delivered a maximum PCE of 7.93% (P2) and 7.43% (P3) with high open-circuit voltage (V_{oc}) of 0.82 and 1.00 V, respectively, in BHJ OSCs, which outperformed the P1-based device with the PCE of 4.35%. It is worth mentioning that the PCEs of 7.93% and 7.43% with high V_{oc} of 0.81 and 1.00 V would definitely be suitable candidates for tandem solar cell fabrication to boost PCE in BHJ OSCs. Overall, the current approach of regulation of side-chain fluorination of conjugated polymers enables us to develop highly efficient multifunctional conjugated polymers with high performance dopant-free PSCs and BHJ OSCs with long-term ambient stability. To the best our knowledge, this is one of the best reports where a set of multifunctional side-chain fluorinated π-conjugated polymers show their compatibility as HTMs in dopant-free PSCs and as photoactive donors in BHJ OSCs with high performance and long-term stability.

RESULTS AND DISCUSSION

The molecular structures of P1−P3, absorption coefficient spectra, and energy level diagram are presented in Figure 1. The thermal properties were determined by probing thermogravimetric analysis (TGA) and differential scanning calorimetry (DSC), and their representative TGA and DSC curves are shown in Figure S1 (Supporting Information (SI)). P1−P3 showed high thermal decomposition temperatures (Table S1, SI) over 400 °C without any characteristic phase transition in the DSC profiles. Further, Figure S2 (SI) shows the normalized UV−visible absorption spectra of P1−P3 in the solution and film states. In addition, P2 and P3 showed more pronounced vibronic shoulders than that of P1, which suggests enhanced inter/intramolecular interactions in the fluorinated polymers. Moreover, P2 and P3 showed gradual improvement (Figure S3, SI) in their vibronic shoulder as the concentration was increased. The incomplete disappearance (Figure S4, SI) of the shoulders at high temperatures may be due to the presence of strong interactions attributed to their enhanced planar structures, which are well correlated with reduced steric hindrance between the D and A units of P1−P3 (*vide infra*). Also, we performed FTIR for P1−P3 to analyze the reason for improved intermolecular interactions in FTIR. However, we found identical FTIR spectra for all the three polymers (Figure S5, SI). The electrochemical properties were estimated from cyclic voltammetry (CV) (Figure S6, SI). The fluorinated polymers P2 and P3 showed deeper highest occupied molecular orbitals (HOMOs) (−5.43 and −5.50 eV) and higher lowest unoccupied molecular orbitals (LUMOs) (−3.61 and −3.68 eV) compared to nonfluorinated polymer P1 (−5.41 and −3.59 eV), respectively, without altering their optical band gaps. This clearly indicates that our approach of regulation of fluorine content on the side chain significantly alters the energy levels without altering the band gaps. Further, the experimental HOMOs and LUMOs were well correlated with density functional theory (DFT) results for the repeating units of P1−P3, as shown in Figure S7 (SI). Next, we also measured ultraviolet photoelectron spectroscopy (UPS) for P1−P3 polymers to estimate the accurate energy levels. The obtained UPS results (Figure S8, SI) are very well correlated with the CV and DFT results. Interestingly, the reduced dihedral angle (θ3) between D and A units (Figure S9 and Table S2, SI) of P2 and P3 may have afforded a better planar structure than that of nonfluorinated P1, which was clearly correlated with the presence of vibronic shoulders at elevated temperatures. Furthermore, higher dipole moments were observed for P2 and P3 (4.44 and 2.75 D), which thus could show a more closely packed structure with greater molecular ordering[31] compared to that of P1 with low dipole moment (1.44 D).

DOI: 10.1021/acsami.7b09146
ACS Appl. Mater. Interfaces 2017, 9, 36053−36060

The impact of degree of side-chain fluorination on the photovoltaic properties of PSCs was analyzed by fabricating dopant-free PSCs in a planar device structure (FTO/blocking TiO_2/mesoporous TiO_2/perovskite/HTM/Ag), and P1−P3 were used as HTMs (Figure 2a). P1−P3 showed very good compatibility in dopant-free PSCs and delivered maximum PCEs of 9.80, 14.94, and 10.35%, respectively. Moreover, all three polymers showed higher performance than dopant-free spiro-OMeTAD-based devices (PCE = 8.74%). It is worth to remind that the obtained PCE of 14.94% is one of the best performances reported in dopant-free polymer HTM-based PSCs (Table S3, SI). The optimized photovoltaic properties of the P1−P3-based PSCs are extracted in Table 1, and the respective current density−voltage (J−V) and external quantum efficiency (EQE) curves are shown in Figure 2b,c. P2- and P3-based devices showed enhanced PCE compared to P1-based devices, which demonstrates the importance of the degree of fluorine content in the side chain for regulating the photovoltaic properties. To provide an insight into the hole transfer process, flash photolysis time-resolved microwave conductivity (TRMC) evaluations[32] were performed for the quartz/mesoporous-TiO_2/perovskite with/without P1−P3 (Figure S10 and Table S4, SI). The highest hole transfer yield (η_{sat}) of 0.88 in the saturated region (ca. 3 μs) was found for P1, followed by P2 (0.80) and P3 (0.54). The delayed hole transfer rates (k) are P1: 8.5×10^6/s, P2: 2.6×10^6/s, and P3: 7.9×10^5/s, respectively. Notably, both η_{sat} and k are increased with the increase of the HOMO levels, indicating that the hole transfer process is mostly governed by the energetic offset. The highest PCE observed for P2 is a result of the most balanced efficiencies of hole transfer at the perovskite/HTM interface and hole transport in HTM associated with a hole mobility. The enhanced short-circuit current density (J_{sc}) of the P2- and P3-based devices could be due to the high space-charge-limited current (SCLC) hole mobility (μ_h) of P2 (9.32×10^{-5} cm^2 V^{-1} s^{-1}) and P3 (4.06×10^{-5} cm^2 V^{-1} s^{-1}) compared to that of P1 (2.51×10^{-5} cm^2 V^{-1} s^{-1}) (Figure S11a, SI). To further describe the improved fill factor (FF) of the P2-based PSCs, the J−V characteristics of the PSCs were measured in the dark under ambient conditions at ±1.5 V (Figure S11b, SI). The rectification ratios of P1−P3-based PSCs were 8.94×10^2, 6.20×10^3, and 2.01×10^3, respectively. Thus, the P2-based PSCs exhibited a sufficiently increased shunt resistance (R_{sh}) and decreased series resistance (R_s), indicating a reduction in the leakage current and more charge extraction/transport efficiency.[19,33] Further, the HTMs with enhanced π−π stacking may be beneficial for providing a much smoother and higher quality film to improve the J_{sc}, FF, and device performance while also prolonging the device lifetime.[34] The atomic force microscopy (AFM) images of pristine polymers (P1−P3) and perovskite:HTM (P1−P3) blends displayed in Figure S12 (SI) and the root-mean-square (RMS) roughness values of pristine polymers (P1 = 2.46 nm, P2 = 1.62 nm, and P3 = 1.81 nm) and composite films of perovskite: P1 = 12.43 nm, perovskite: P2 = 5.40 nm, and perovskite: P3 = 6.21 nm are well supporting the aforementioned claims. Further, steady-state photoluminescence (PL) (Figure S13, SI) of perovskite, perovskite: P1, perovskite: P2, and perovskite: P3 confirmed that the charge separation at perovskite/dopant-free HTMs is very well correlated with the photovoltaic properties of P1−P3-based PSCs.[16] Electrochemical impedance spectroscopy (EIS) measurements were performed on the P1−P3-based PSCs to characterize their hole/charge transport behavior (Figure S14, SI). The previously reported equivalent circuit model was used to fit the obtained EIS curves.[19] Therefore, a recombination

Table 1. Photovoltaic Properties of P1−P3-Based Dopant-Free PSCs

HTM	scan	J_{sc} (mA/cm^2)	V_{OC} (V)	FF (%)	PCE$_{max}$ (%)	calcd J_{sc} (mA/cm^2)[a]
P1	reverse	17.85	1.00	54.66	9.80	18.62
P1	forward	17.11	0.97	54.32	9.08	18.62
P2	reverse	20.17	1.04	70.65	14.94	20.23
P2	forward	19.69	1.04	68.17	14.06	20.23
P3	reverse	18.58	1.03	53.81	10.35	19.48
P3	forward	19.56	1.01	50.80	10.12	19.48
ref[b]	reverse	19.58	1.01	43.91	8.74	18.47

[a]Calculated J_{sc} from EQE. [b]Spiro-oMeTAD-based PSCs in dopant-free conditions.

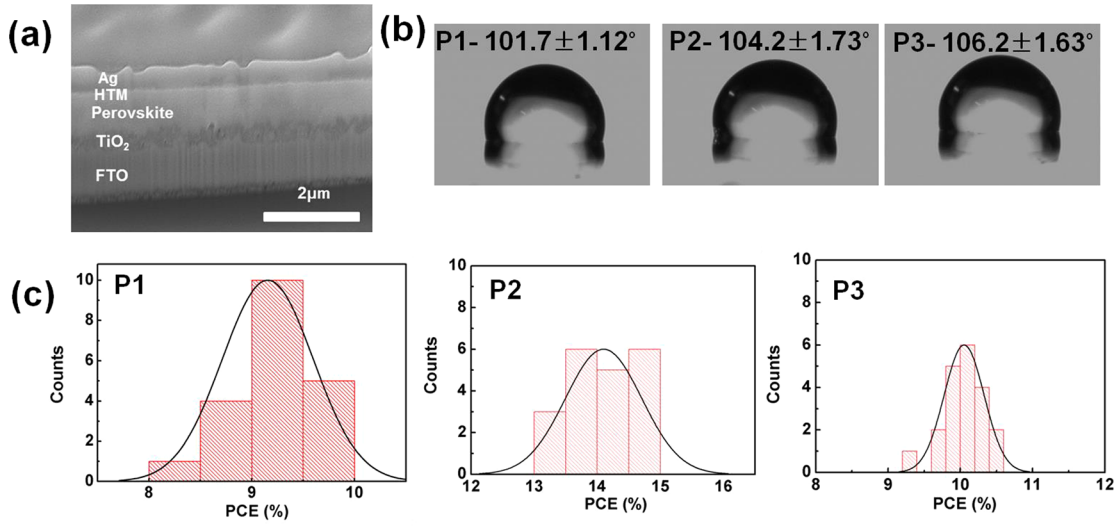

Figure 3. (a) SEM cross-section image of P2-based PSCs. (b) Water contact angles of P1−P3. (c) Histograms of the PCE values of the P1−P3-based PSCs.

DOI: 10.1021/acsami.7b09146
ACS Appl. Mater. Interfaces 2017, 9, 36053−36060

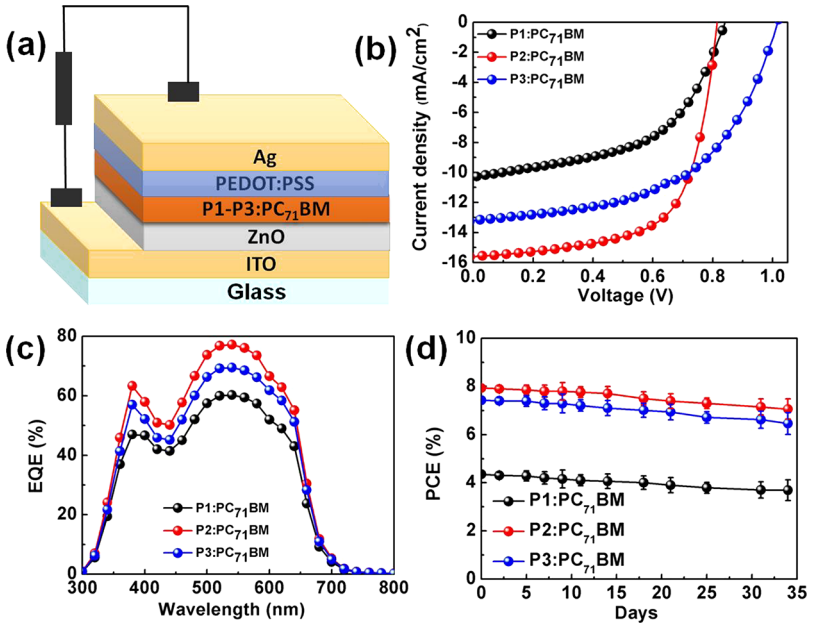

Figure 4. (a) Device structure of BHJ IOSCs. (b) $J-V$ curves of P1−P3:$PC_{71}BM$-based BHJ OSCs. (c) EQE curves of P1−P3:$PC_{71}BM$-based BHJ OSCs. (d) Stability of P1−P3:$PC_{71}BM$-based BHJ OSCs.

loss process was confirmed at low frequency, while the high frequency was related to the diffusion of holes via HTMs. The recombination rate is inversely proportional to the recombination resistance (R_{rec}, extracted from EIS curve), which itself follows an exponential decrease with increasing applied voltage.[35] The R_{rec} decreased in the order of P2 > P3 > P1 at low and high voltages, which gave a longer charge carrier lifetime for better transport for P2 and P3 HTM-based PSCs, thereby improving the performance of the PSCs.

Furthermore, the hole conductivity (σHTM) increased with increasing voltage, due to the higher gradient of hole density in HTM caused by the hole injection from the perovskite layer.[35]As a result, the conductivity findings of P1−P3 agreed well with the dopant-free PSC device performances. Further, the durability of the new HTM-based dopant-free PSCs was analyzed under ambient condition (Figure 2d). All three dopant-free PSCs retained more than 75% of their initial efficiency after exposure to air for over 30 days (720 h) due to the enhanced hydrophobic nature of the polymers and to the high quality pinhole-free films (Figure 3a). Thus, P1−P3 are showing far better stability in PSCs than spiro-OMeTAD-based dopant-free PSC devices. In particular, P2 and P3 showed high sustainability of PCE over 30 days due to their higher hydrophobicity (water contact angle of 104.2° and 106.2°) which effectively reduced the water penetration compared to that of P1 (101.7°) (Figure 3b). The histograms of the P1−P3-based dopant-free PSCs shown in Figure 3c clearly show the reproducibility of dopant-free PSCs with minimal hysteresis.

Next, the P1−P3-based BHJ OSCs were fabricated in inverted (ITO/ZnO/P1−P3:$PC_{71}BM$/PEDOT:PSS/Ag) configuration to understand the same effect (Figure 4a). The optimized device fabrication procedure is shown in the Supporting Information. The $J-V$ and EQE curves of the optimized devices are shown in Figure 4b,c, and the photovoltaic parameters are summarized in Table 2. Especially, the fluorinated polymer (P2 and P3)-based BHJ OSCs showed enhanced PCEs of 7.93% and 7.43% compared to P1-based devices (4.35%). This enhanced PCE of the P2- and P3-based

Table 2. Photovoltaic Properties of P1−P3-Based BHJ OSCs

blend	J_{sc} (mA/cm^2)	V_{OC} (V)	FF (%)	PCE_{max} (%)	calcd J_{sc} (mA/cm^2)[a]
P1: $PC_{71}BM$	9.96	0.81	53.79	4.35	9.86
P2: $PC_{71}BM$	15.10	0.82	64.23	7.93	15.23
P3: $PC_{71}BM$	13.25	1.00	55.57	7.43	13.25

[a]Calculated J_{sc} from EQE.

devices strongly correlated with their synergistic improvement in J_{sc} and FF values compared to that of P1-based devices. The high open-circuit voltage (V_{oc}) of P2- and P3-based devices over P1 can be understood from the deep HOMOs of P2 and P3. More importantly, the enhanced J_{sc} and FF for P2 (J_{sc} = 15.10 mA/cm^2, FF = 64.23%) and P3 (J_{sc} = 13.25 mA/cm^2, FF = 55.57%) based BHJ OSCs compared to that for P1 (J_{sc} = 9.96 mA/cm^2, FF = 53.79%) is the major reason for the enhanced PCE for the fluorinated polymers. The improved J_{sc} values for the P2- and P3-based devices could be due to their higher absorption coefficients (5.5×10^4 and 4.8×10^4 M^{-1} cm^{-1}) than for P1 (3.8×10^4 M^{-1} cm^{-1}). Further, these enhanced J_{sc} values for the P2- and P3-based BHJ OSCs are very consistent with their strong EQE responses of up to ~77% and 70%, respectively, compared to the lower spectral response of the P1-based devices (59%), as shown in Figure 4c. The J_{sc} values were well matched with the J_{sc} values calculated from the EQE spectra. In addition, the P2- and P3-based BHJ OSCs showed improved FF compared to P1-based BHJ OSCs, which was attributed to the reduced series resistance. Further, the improved J_{sc} and FF for the P2- and P3-based BHJ OSCs are well aligned with their improved SCLC charge transport properties compared to those of the P1-based BHJ OSCs. As shown in Figure S15 and Table S5 (SI), P2:$PC_{71}BM$ and P3:$PC_{71}BM$ blends showed higher μ_h (1.81×10^{-3} and 1.37×10^{-3} cm^2 V^{-1} s^{-1}) and electron mobility values (μ_e = 9.23×10^{-4} and 5.63×10^{-4} cm^2 V^{-1} s^{-1}) than P1:$PC_{71}BM$ blends (μ_h

DOI: 10.1021/acsami.7b09146
ACS Appl. Mater. Interfaces 2017, 9, 36053−36060

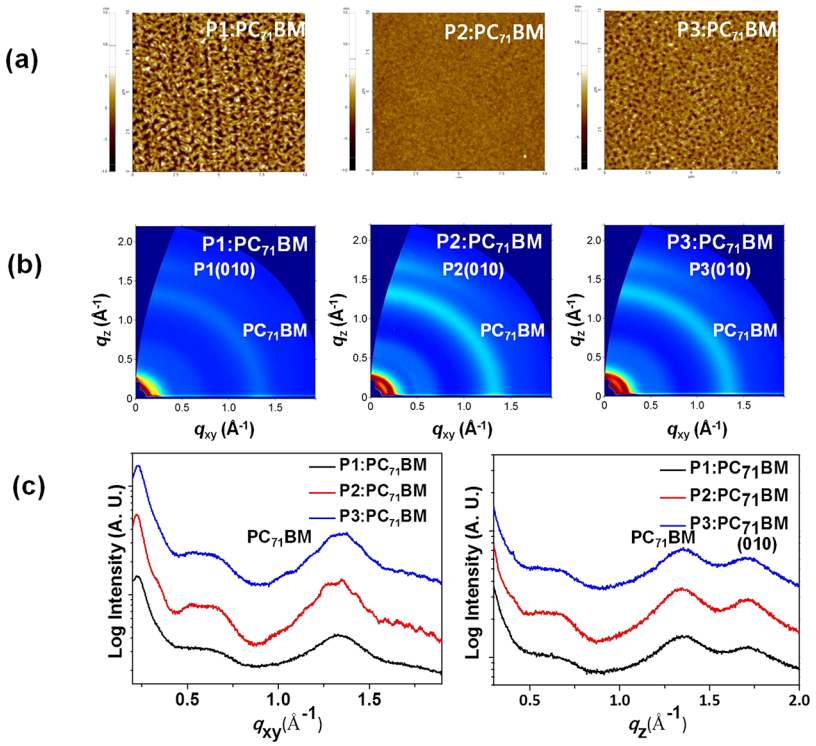

Figure 5. (a) AFM images of the optimized P1−P3: $PC_{71}BM$ blends. (b) 2D-GIWAXS patterns of the P1−P3: $PC_{71}BM$ BHJ blends. (c) In-plane linecut (q_{xy}) and out-of-plane linecut (q_z) of 2D-GIWAXS images.

$= 8.40 \times 10^{-4}$; $\mu_e = 2.35 \times 10^{-4}$ cm^2 V^{-1} s^{-1}). The ambient stability of photoactive materials is an essential factor for the practical use of BHJ OSCs. Hence, we also studied the ambient stability (Figure 4d) for the BHJ OSCs and found that they showed high ambient stability over 30 days (720 h) with maximum retention of their initial photovoltaic properties. The improved stability was attributed to the inverted device structure and stable morphological properties of the blends.[36]

The active layer morphology of the P1−P3-based optimized devices was analyzed by atomic force microscopy (AFM), as shown in Figure 5a. The fluorinated polymer blends showed enhanced miscibility with $PC_{71}BM$ and displayed relatively smooth surface morphology with a RMS of 0.46 (P2) and 1.21 nm (P3). In comparison, the nonfluorinated P1 and $PC_{71}BM$ blends had the phase-separated morphology with larger domain spacing and RMS roughness of 2.26 nm. Next, we examined the effect of the fluorination on the polymer packing structure and its orientation in thin films, which significantly affect the charge transport in the thin film. The polymer blends were investigated by two-dimensional grazing incidence X-ray scattering (2D-GIWAXS) measurements (Figure 5b,c). All three blend films showed a similar (100) peak of the polymer donors at q_{xy} = 0.22 $Å^{-1}$ (2.86 nm) and a broad peak from $PC_{71}BM$ at q_{xy} = 1.33 $Å^{-1}$ (0.47 nm) in the in-plane direction. Also, all three polymer films had the $\pi-\pi$ stacking (010) peak of the polymers at q_{xy} = 1.68 $Å^{-1}$ (0.37 nm) in the out-of-plane direction, showing the preferential face-on orientation.[37−39] However, it was evident that the fluorinated polymers P2 and P3 had much stronger $\pi-\pi$ stacking peak as shown in Figure 5b,c. This feature suggested that the fluorination of the polymers successfully promoted the formation of the well-organized intermolecular assembly, which is well correlated with their improved charge transport characteristics in the case of dopant-free PSCs. The P2 and P3 blends had well-developed, face-on oriented assembly of polymers and suitable BHJ morphology with large interfacial area, which produced efficient exciton dissociation and vertical charge transport between the electrodes, which collectively led to the enhanced PCE values for the P2- and P3-based devices.

CONCLUSIONS

In summary, we successfully demonstrated a series of multifunctional π-conjugated polymers by regulating the degree of side-chain fluorination. The multifunctional π-conjugated polymers (P1−P3) showed an excellent compatibility as HTM in dopant-free PSCs and as photoactive donors in BHJ OSCs. Especially, the fluorinated polymer (P2 and P3) based devices exhibited much higher PCE values of 14.94% and 10.35% than P1-based devices (PCE value of 9.80%) in dopant-free PSCs. Particularly, the high PCE values of the P2- and P3-based devices were attributed to the enhanced charge transport via improved face-on $\pi-\pi$ stacking, packing, and quality film formation of the polymers and better aligned energy levels with respect to the perovskite. Further, a similar trend was observed in BHJ OSCs, highlighting the importance of the present approach for developing multifunctional π-conjugated polymers by the regulating the side-chain fluorination. Especially, P2 and P3 based BHJ OSCs showed improved PCE of 7.93% and 7.43% compared to P1 (PCE = 4.35%). The obtained results were highly correlated with their maximized absorption coefficients, balanced charge transport properties, and reduced recombination losses, which were collectively accomplished via improved inter/intramolecular interactions, well-developed BHJ morphology, and face-on oriented polymer packing structures. In addition to their enhanced performance, the P1−P3-based dopant-free PSCs and BHJ OSCs also demonstrated an excellent long-term ambient stability over 30 days (720 h), which further confirmed the potential behavior of new

DOI: 10.1021/acsami.7b09146
ACS Appl. Mater. Interfaces 2017, 9, 36053−36060

multifunctional π-conjugated polymers toward stable and scalable photovoltaic devices.

■ ASSOCIATED CONTENT

Supporting Information

The Supporting Information is available free of charge on the ACS Publications website at DOI: 10.1021/acsami.7b09146.

Additional text describing materials and characterization, specific device fabrication, and detailed synthetic procedure; scheme-1 showing synthetic route for polymers, 15 figures showing thermal gravimetric analysis, differential scanning calorimetry, concentration-dependent and temperature-dependent UV−vis spectra, FTIR, CV, DFT simulations, UPS, TRMS plots, SCLC, dark *J*−*V* curves of PSCs, AFM images, steady state PL and EIS data. Five tables showing preliminary characteristics, dihedral angles, literature on dopant-free PSCs, TRMS results, and SCLC mobility data (PDF)

■ AUTHOR INFORMATION

Corresponding Authors

*E-mail: hyunjung@kookmin.ac.kr (H. L.).
*E-mail: saeki@chem.eng.osaka-u.ac.jp (A. S.).
*E-mail: shjin@pusan.ac.kr (S.-H. J.). Telephone: +82 51 510 2727. Fax: +82 51 581 2348.
*E-mail: smk1017@kims.re.kr (M. S.). Telephone: +82-55-280-3686. Fax: +82-55-280-3570.

ORCID

Akinori Saeki: 0000-0001-7429-2200
Sung-Ho Jin: 0000-0001-6631-983X
Myungkwan Song: 0000-0001-7935-5303

Notes

The authors declare no competing financial interest.

■ ACKNOWLEDGMENTS

This study was supported by the New & Renewable Energy Core Technology Program of the Korea Institute of Energy Technology Evaluation and Planning (KETEP), granted financial resource from the Ministry of Trade, Industry & Energy (No. 20143030011560), Republic of Korea.

■ REFERENCES

(1) Yu, Z.; Sun, L. Recent Progress on Hole-Transporting Materials for Emerging Organometal Halide Perovskite Solar Cells. *Adv. Energy Mater.* **2015**, *5*, 1500213.

(2) Kojima, A.; Teshima, K.; Shirai, Y.; Miyasaka, T. Organometal Halide Perovskites as Visible-Light Sensitizers for Photovoltaic Cells. *J. Am. Chem. Soc.* **2009**, *131*, 6050−6051.

(3) Choi, H.; Mai, C.-K.; Kim, H.-B.; Jeong, J.; Song, S.; Bazan, G. C.; Kim, J. Y.; Heeger, A. J. Conjugated Polyelectrolyte Hole Transport layer for Inverted-Type Perovskite Solar Cells. *Nat. Commun.* **2015**, *6*, 7348.

(4) Ameen, S.; Rub, M. A.; Kosa, S. A.; Alamry, K. A.; Akhtar, M. S.; Shin, H.-S.; Seo, H.-K.; Asiri, A. M.; Nazeeruddin, M. K. Perovskite Solar Cells: Influence of Hole Transporting Materials on Power Conversion Efficiency. *ChemSusChem* **2016**, *9*, 10−27.

(5) Volker, S. F.; Collavini, S.; Delgado, J. L. Organic Charge Carriers for Perovskite Solar Cells. *ChemSusChem* **2015**, *8*, 3012−3028.

(6) Yang, W. S.; Noh, J. H.; Jeon, N. J.; Kim, Y. C.; Ryu, S.; Seo, J.; Seok, S. I. High-Performance Photovoltaic Perovskite Layers Fabricated through Intramolecular Exchange. *Science* **2015**, *348*, 1234−1237.

(7) Jeon, N. J.; Noh, J. H.; Yang, W. S.; Kim, Y. C.; Ryu, S.; Seo, J.; Seok, S. I. Compositional Engineering of Perovskite Materials for High-Performance Solar Cells. *Nature* **2015**, *517*, 476−480.

(8) Liu, Y.; Zhao, J.; Li, Z.; Mu, C.; Ma, W.; Hu, H.; Jiang, K.; Lin, H.; Ade, H.; Yan, H. Aggregation and Morphology Control Enables Multiple Cases of High-Efficiency Polymer Solar Cells. *Nat. Commun.* **2014**, *5*, 5293.

(9) Meng, T.; Liu, C.; Wang, K.; He, T.; Zhu, Y.; Al-Enizi, A.; Elzatahry, A.; Gong, X. High Performance Perovskite Hybrid Solar Cells with E-beam- Processed TiOx Electron Extraction Layer. *ACS Appl. Mater. Interfaces* **2016**, *8*, 1876−1883.

(10) Bi, D.; Tress, W.; Dar, M. I.; Gao, P.; Luo, J.; Renevier, C.; Schenk, K.; Abate, A.; Giordano, F.; Baena, J.-P. C.; Decoppet, J.-D.; Zakeeruddin, S. M.; Nazeeruddin, M. K.; Gratzel, M.; Hagfeldt, A. Efficient Luminescent Solar Cells Based on Tailored Mixed-Cation Perovskites. *Sci. Adv.* **2016**, *2*, 1501170.

(11) Yao, H.; Ye, L.; Zhang, H.; Li, S.; Zhang, S.; Hou, J. Molecular Design of Benzodithiophene-Based Organic Photovoltaic Materials. *Chem. Rev.* **2016**, *116*, 7397−7457.

(12) Liu, Y.; Hong, Z.; Chen, Q.; Chen, H.; Chang, W.-H.; Yang, Y. M.; Song, T.-B.; Yang, Y. Perovskite Solar Cells Employing Dopant-Free Organic Hole Transport Materials with Tunable Energy Levels. *Adv. Mater.* **2016**, *28*, 440−446.

(13) Zhang, F.; Yi, C.; Wei, P.; Bi, X.; Luo, J.; Jacopin, G.; Wang, S.; Li, X.; Xiao, Y.; Zakeeruddin, S. M.; Gratzel, M. A Novel Dopant-Free Triphenylamine Based Molecular "Butterfly" Hole-Transport Material for Highly Efficient and Stable Perovskite Solar Cells. *Adv. Energy Mater.* **2016**, *6*, 1600401.

(14) Malinkiewicz, O.; Yella, A.; Lee, Y. H.; Espallargas, G. M.; Grätzel, M.; Nazeeruddin, M. K.; Bolink, H. J. Perovskite Solar Cells Employing Organic Charge-Transport Layers. *Nat. Photonics* **2014**, *8*, 128−132.

(15) Kim, G.-W.; Kim, J.; Lee, G.-Y.; Kang, G.; Lee, J.; Park, T. A Strategy to Design a Donor−π−Acceptor Polymeric Hole Conductor for an Efficient Perovskite Solar Cell. *Adv. Energy Mater.* **2015**, *5*, 1500471.

(16) Liao, H.-C.; Dexter Tam, T. L.; Guo, P.; Wu, Y.; Manley, E. F.; Huang, W.; Zhou, N.; Soe, C. M. M.; Wang, B.; Wasielewski, M. R.; Chen, L. X.; Kanatzidis, M. G.; Facchetti, A.; Chang, R. P. H.; Marks, T. J. Dopant-Free Hole Transporting Polymers for High Efficiency Environmentally Stable Perovskite Solar Cells. *Adv. Energy Mater.* **2016**, *6*, 1600502.

(17) Ryu, S.; Noh, J. H.; Jeon, N. J.; Kim, Y. C.; Yang, W. S.; Seo, J.; Seok, S. I. Voltage Output of Efficient Perovskite Solar Cells with High Open-Circuit Voltage and Fill factor. *Energy Environ. Sci.* **2014**, *7*, 2614−2618.

(18) Zhao, D.; Sexton, M.; Park, H.-Y.; Baure, G.; Nino, J. C.; So, F. High-Efficiency Solution-Processed Planar Perovskite Solar Cells with a Polymer Hole Transport Layer. *Adv. Energy Mater.* **2015**, *5*, 1401855.

(19) Reddy, S. S.; Gunasekar, K.; Heo, J. H.; Im, S. H.; Kim, C. S.; Kim, D.-H.; Lee, J. Y.; Song, M.; Jin, S.-H. Highly Efficient Organic Hole Transporting Materials for Perovskite and Organic Solar Cells with Long-Term Stability. *Adv. Mater.* **2016**, *28*, 686−693.

(20) Li, Z.; Zhu, Z.; Chueh, C.-C.; Jo, S. B.; Luo, J.; Jang, S.-H.; Jen, A. K.-Y. Rational Design of Dipolar Chromophore as an Efficient Dopant-Free Hole-Transporting Material for Perovskite Solar Cells. *J. Am. Chem. Soc.* **2016**, *138*, 11833−11839.

(21) Yun, J. H.; Park, S.; Heo, J. H.; Lee, H.-S.; Yoon, S.; Kang, J.; Im, S. H.; Kim, H.; Lee, W.; Kim, B. S.; Ko, M. J.; Chung, D. S.; Son, H. J. Enhancement of Charge Transport Properties of Small Molecule Semiconductors by Controlling Fluorine Substitution and Effects on Photovoltaic Properties of Organic Solar Cells and Perovskite Solar Cells. *Chem. Sci.* **2016**, *7*, 6649−6661.

(22) Qin, P.; Tetreault, N.; Dar, M. I.; Gao, P.; McCall, K. L.; Rutter, S. R.; Ogier, S. D.; Forrest, N. D.; Bissett, J. S.; Simms, M. J.; Page, A. J.; Fisher, R.; Gratzel, M.; Nazeeruddin, M. K. A Novel Oligomer as a Hole Transporting Material for Efficient Perovskite Solar Cells. *Adv. Energy Mater.* **2015**, *5*, 1400980.

DOI: 10.1021/acsami.7b09146
ACS Appl. Mater. Interfaces 2017, 9, 36053−36060

(23) Liu, D.; Yang, J.; Kelly, T. L. Compact Layer Free Perovskite Solar Cells with 13.5% Efficiency. *J. Am. Chem. Soc.* **2014**, *136*, 17116−17122.
(24) Heo, J. H.; Im, S. H.; Noh, J. H.; Mandal, T. N.; Lim, C.-S.; Chang, J. A.; Lee, Y. H.; Kim, H.-J.; Sarkar, A.; Nazeeruddin, M. K.; Gratzel, M.; Seok, S. I. Efficient Inorganic−Organic Hybrid Heterojunction Solar Cells Containing Perovskite Compound and Polymeric Hole Conductors. *Nat. Photonics* **2013**, *7*, 486−491.
(25) Li, X.; Liu, X.; Wang, X.; Zhao, L.; Jiu, T.; Fang, J. Polyelectrolyte Based Hole-Transporting Materials for High Performance Solution Processed Planar Perovskite Solar Cells. *J. Mater. Chem. A* **2015**, *3*, 15024−15029.
(26) Matsui, T.; Petrikyte, I.; Malinauskas, T.; Domanski, K.; Daskeviciene, M.; Steponaitis, M.; Gratia, P.; Tress, W.; Correa-Baena, J.-P.; Abate, A.; Hagfeldt, A.; Gratzel, M.; Nazeeruddin, M. K.; Getautis, V.; Saliba, M. Additive-Free Transparent Triarylamine-Based Polymeric Hole-Transport Materials for Stable Perovskite Solar Cells. *ChemSusChem* **2016**, *9*, 2567−2571.
(27) Kim, G.-W.; Kang, G.; Kim, J.; Lee, G.-Y.; Kim, H. I.; Pyeon, L.; Lee, J.; Park, T. Dopant-Free Polymeric Hole Transport Materials for Highly Efficient and Stable Perovskite Solar Cells. *Energy Environ. Sci.* **2016**, *9*, 2326−2333.
(28) Kranthiraja, K.; Gunasekar, K.; Kim, H.; Cho, A.-N.; Park, N.-G.; Kim, S.; Kim, B. J.; Nishikubo, R.; Saeki, A.; Song, M.; Jin, S.-H. High-Performance Long-Term-Stable Dopant-Free Perovskite Solar Cells and Additive-Free Organic Solar Cells by Employing Newly Designed Multirole π-Conjugated Polymers. *Adv. Mater.* **2017**, *29*, 1700183.
(29) Son, H. J.; Wang, W.; Xu, T.; Liang, Y.; Wu, Y.; Li, G.; Yu, L. Synthesis of Fluorinated Polythienothiophene-co-benzodithiophenes and Effect of Fluorination on the Photovoltaic Properties. *J. Am. Chem. Soc.* **2011**, *133*, 1885−1894.
(30) Oh, J.; Kranthiraja, K.; Lee, C.; Gunasekar, K.; Kim, S.; Ma, B.; Kim, B. J.; Jin, S.-H. Side-Chain Fluorination: An Effective Approach to Achieving High-Performance All-Polymer Solar Cells with Efficiency Exceeding 7%. *Adv. Mater.* **2016**, *28*, 10016−10023.
(31) Jo, J. W.; Jung, J. W.; Wang, H.-W.; Kim, P.; Russell, T. P.; Jo, W. H. Fluorination of Polythiophene Derivatives for High Performance Organic Photovoltaics. *Chem. Mater.* **2014**, *26*, 4214−4220.
(32) Ishida, N.; Wakamiya, A.; Saeki, A. Quantifying Hole Transfer Yield from Perovskite to Polymer Layer: Statistical Correlation of Solar Cell Outputs with Kinetic and Energetic Properties. *ACS Photonics* **2016**, *3*, 1678−1688.
(33) Li, N.; Lassiter, B. E.; Lunt, R. R.; Wei, G.; Forrest, S. R. Open circuit voltage enhancement due to reduced dark current in small molecule photovoltaic cells. *Appl. Phys. Lett.* **2009**, *94*, 023307.
(34) Fabregat-Santiago, F.; Garcia-Belmonte, G.; Mora-Sero, I.; Bisquert, J. Characterization of Nanostructured Hybrid and Organic Solar Cells by Impedance Spectroscopy. *Phys. Chem. Chem. Phys.* **2011**, *13*, 9083−9118.
(35) Teh, C.-H.; Daik, R.; Lim, E.-L.; Yap, C. C.; Ibrahim, M. A.; Ludin, N. A.; Sopian, K.; Teridi, M. S. M. A Review of Organic Small Molecule-Based Hole-Transporting Materials for Meso-Structured Organic−Inorganic Perovskite Solar Cells. *J. Mater. Chem. A* **2016**, *4*, 15788−15822.
(36) Holliday, S.; Ashraf, R. S.; Wadsworth, A.; Baran, D.; Yousaf, S. A.; Nielsen, C. B.; Tan, C.-H.; Dimitrov, S. D.; Shang, Z.; Gasparini, N.; Alamoudi, M.; Laquai, F.; Brabec, C. J.; Salleo, A.; Durrant, J. R.; McCulloch, I. High-Efficiency and Air-Stable P3HT-Based Polymer Solar Cells with a New Non-Fullerene Acceptor. *Nat. Commun.* **2016**, *7*, 11585.
(37) Lee, C.; Kang, H.; Lee, W.; Kim, T.; Kim, K.-H.; Woo, H. Y.; Wang, C.; Kim, B. J. High-Performance All-Polymer Solar Cells Via Side-Chain Engineering of the Polymer Acceptor: The Importance of the Polymer Packing Structure and the Nanoscale Blend Morphology. *Adv. Mater.* **2015**, *27*, 2466−2471.
(38) Kang, H.; Uddin, M. A.; Lee, C.; Kim, K.-H.; Nguyen, T. L.; Lee, W.; Li, Y.; Wang, C.; Woo, H. Y.; Kim, B. J. Determining the Role of Polymer Molecular Weight for High-Performance All-Polymer Solar Cells: Its Effect on Polymer Aggregation and Phase Separation. *J. Am. Chem. Soc.* **2015**, *137*, 2359−2365.
(39) Oesinghaus, L.; Schlipf, J.; Giesbrecht, N.; Song, L.; Hu, Y.; Bein, T.; Docampo, P. Müller-Buschbaum, P. Toward Tailored Film Morphologies: The Origin of Crystal Orientation in Hybrid Perovskite Thin Films. *Adv. Mater. Interfaces* **2016**, *3*, 1600403.

DOI: 10.1021/acsami.7b09146
ACS Appl. Mater. Interfaces 2017, 9, 36053−36060